Computers and Concrete, *Vol. 25, No. 4* (*2020*) *293-302*
DOI: https://doi.org/10.12989/cac.2020.25.4.293

Cyclic performance of RC beam-column joints enhanced with superelastic SMA rebars

Amirhosein Ghasemitabar[a], Javad Mokari Rahmdel* and Erfan Shafei[b]

Faculty of Civil Engineering, Urmia University of Technology, Urmia, Iran

(*Received October 17, 2019, Revised February 12, 2020, Accepted February 20, 2020*)

Abstract. Connections play a significant role in strength of structures against earthquake-induced loads. According to the post-seismic reports, connection failure is a cause of overall failure in reinforced concrete (RC) structures. Connection failure results in a sudden increase in inter-story drift, followed by early and progressive failure across the entire structure. This article investigated the cyclic performance and behavioral improvement of shape-memory alloy-based connections (SMA-based connections). The novelty of the present work is focused on the effect of shape memory alloy bars is damage reduction, strain recoverability, and cracking distribution of the stated material in RC moment frames under seismic loads using 3D nonlinear static analyses. The present numerical study was verified using two experimental connections. Then, the performance of connections was studied using 14 models with different reinforcement details on a scale of 3:4. The response parameters under study included moment-rotation, secant stiffness, energy dissipation, strain of bar, and moment-curvature of the connection. The connections were simulated using LS-DYNA environment. The models with longitudinal SMA-based bars, as the main bars, could eliminate residual plastic rotations and thus reduce the demand for post-earthquake structural repairs. The flag-shaped stress-strain curve of SMA-based materials resulted in a very slight residual drift in such connections.

Keywords: beam-column panel zone; reinforced concrete; SMA-based materials; energy dissipation; residual drift

1. Introduction

The importance of structural connections lies in their responsibility for appropriate transfer of loads created in the elements connected to them. In structural systems with ductile moment frames, connections play a significant role in the frame behavior and thus any change in the stiffness or strength of these connections significantly affects the frame’s lateral load-bearing capacity. Connection failure during an earthquake may lead to a sudden increase in inter-story drift and risk of structural failure due to the increased P-Δ effect. As a result, inconsiderate design and poor compliance with constructional details of connections with ductile moment frames are regarded as a structural fault. The base of seismic design is set to enable structures to resist moderate earthquakes undamaged, survive strong earthquakes without experiencing serious damages as it is predicted in the structure's effective lifespan, and prevent the overall collapse in very strong earthquakes (Ha *et al.* 1992, El-Amoury and Ghobarah 2002).

The behavior of traditional beam-column joints is efficiently investigated considering RC frame structures having wide (also called flexible or flat) beams (Masi and Santarsiero 2013), which are widely used in the European residential building stock. Wide experimental investigations are conducted on full scale beam-column joints with wide beam and the main results of tests are reported and discussed. In addition, the role of different earthquake resistant design levels on joint performances is pointed out. Furthermore, a recent study proposes simple strengthening solutions made by fiber reinforced polymers (FRP) systems able to effectively improve seismic capacity through feasible arrangement suitable in case a wide beam (Santarsiero 2018). Detailed nonlinear finite element models were calibrated based on experiments. An FRP strengthening intervention based on a brand new arrangement was modeled in order to perform additional simulations under seismic actions. Another study presented a numerical framework simulating the fatigue performance of hybrid FRP (HFRP) strengthened RC beam (Wang *et al.* 2020). Beams are pre-cracked first, then strengthened by HFRP, and subjected to fatigue loading. The test variable is the pre-stress of HFRP. Stress distribution and damage development of pre-cracking, strengthening and fatigue loading process are analyzed. The user-subroutine UMAT in Abaqus is used for implementation of the constitutive models of component materials. The formation of a plastic hinge at the concrete column-beam connection suddenly reduces structural stability and energy absorption, which leads to a progressive failure. This phenomenon opposes seismic design philosophy and should be strongly avoided. Another state of plastic hinge formation is its development in columns and extending to the panel zone. This type of connections reduces structural ductility lower than the acceptable design level. Investigating and improving the

*Corresponding author, Assistant Professor
E-mail: j.mokari@uut.ac.ir
[a]Ms.c.
E-mail: a.ghasemitabar@civil.uut.ac.ir
[b]Associate Professor
E-mail: e.shafei@uut.ac.ir

http://www.techno-press.org/?journal=cac&subpage=8
ISSN: 1598-8198 (Print), 1598-818X (Online)

seismic behavior of these connections using modern materials are an important topic in the enhancement of structural behavior of concrete. Among these materials are SMAs, which offer superelastic capabilities and are capable of resisting large deformations and returning to their initial shape without loss of resistance. Additionally, these materials can eliminate residual strains (Youssef 2008, DesRoches *et al*. 2004, Qissab and Salman 2018). As reported in literature, SMA bars benefit from superelastic performance and can resist high loads without residual strains. For instance, Azariani *et al*. (2018) conducted experimental study of eight specimens of exterior concrete beam-column joints under reversed cyclic loads with different transverse reinforcements to investigate the effects of concrete confinement. In addition, application of the developed ribbed Fe-SMA bars embedded in a shotcrete layer to strengthen RC structure is also studied (Shahverdi *et al*. 2016). In this way, Georgiades *et al*. (2005) demonstrated the feasibility of using smart GFRP reinforcements to effectively monitor reinforced concrete beams subjected to flexural and creep loads, and developed non-linear numerical models to predict the behavior of these beams.

Youssef *et al*. (2008) investigated the behavior of two SMA-based connections. Both samples were examined in highly seismic areas with moderate ductility, and their drift, plastic rotation, and energy dissipation were studied. Results showed that the SMA bar was capable of eliminating post-yield deformations. As another advantage compared to ordinary connections, this sample experienced slight residual drifts. Masi *et al*. (2013) conducted experimental and numerical investigations on the seismic behavior of external connections by studying four external connection specimens at a full scale. The experiment was performed by applying horizontal drifts above the column. Results showed how an axial load on the column could change the failure and collapse modes. As a result, the failure and load transfer mechanism of the plastic hinge from the beam towards the connection as well as the cracking propagation in this area are strongly dependent on axial loading of the column. Chalioris *et al*. (2008) investigated the external connections by considering reinforcement details in the panel zone. They used *X*-shape bars in this area as the shear reinforcement. Results showed that using *X*-shape bars improves damage modes due to the formation of ductile flexural plastic hinge. In addition, the combination of inclined bars and stirrups considerably improves cyclic behavior and performance of the connections.

The fundamental defect in connections is their inappropriate design in resisting shear loads. Inadequate shear and moment bars in the connection core are two major issues in the design process. These results were obtained from seismic damages in different countries, showing two key modes, namely shear failure and flexural failure in the connection (Hawileh *et al*. 2010). The response mechanism of connections against lateral loads is a combination of a tensile and compressive arm system for transferring shear load of connection in the concrete core. The compressive strut works diagonally due to the reaction of concrete core confined between compressive, tensile, and shear bars. The remaining loads transferred from beam-column bars in the connection core create a truss mechanism, which controls the strength of the diagonal compressive arm and that of the connection after cracking. The concrete is confined by the transversal bars in connections which, in turn, enhances the performance of diagonal compressive strut and increases the connection strength. Excessive shear load results in diagonal concrete cracking, which ultimately leads to concrete crushing in the connection area and causes pinched hysteresis curve-an undesirable behavior-which is difficult to improve after a damage to the connection (Li and Kulkarni 2009).

Furthermore, many research works show that the use of fiber based elements could accurately predict the cyclic response of concrete beam column connections and column connections reinforced with regular steel and superelastic shape memory alloy. In this way, analytical prediction of the seismic behavior of superelastic shape memory alloy reinforced concrete elements is investigated (Alam *et al*. 2008). The seismic performance of concrete columns reinforced with hybrid SMA and fiber reinforced polymer (FRP) bars is analyzed in depth (Billah and Alam 2012). The re-centering phenomenon of SMA RC members is investigated to assess the ability to respond with stable hysteresis and achieve similar strength and ductility to concrete reinforced with conventional deformed bars (Abdulridha 2013). Furthermore, a recent research is conducted to exploit the characteristic of SMA such that concrete Beam-Column Joints (BCJs) reinforced with SMA bars at the plastic hinge region to reduce the residual deformation at the end of earthquakes. (Nehdi *et al*. 2011). Kabir *et al*. (2016) compared the performance characteristics of steel, SMA/steel, glass fiber reinforced polymer (GFRP) and SMA/FRP tested beam-column joints reinforced with different configurations to assess their capacity to endure extreme loading. Alam *et al*. (2012) analytically investigated the effect of SMA as reinforcement in concrete structures for three different stories (3, 6 and 8) reinforced concrete (RC) buildings. For each building, three different reinforcement detailing are considered: (i) steel reinforcement (Steel) only, (ii) SMA rebar used in the plastic hinge region of the beams and steel rebar in other regions (Steel-SMA), and (iii), beams fully reinforced with SMA rebar (SMA) and steel rebar in other regions.

To address the previously discussed limitations in steel reinforcing bars, the authors proposed the idea of using shape memory alloy (SMA) rebar as reinforcement for concrete structures. The proposed reinforcement was sought as a mean to introduce the features of ductility and re-centering to RC structures. A schematic of the newly proposed composite rebar is shown in Fig. 1. The nonlinear, yet pseudo-elastic behavior typical of superelastic SMA fibers will allow the joint to exhibit hysteretic and ductile behavior with minimal damage to the RC frame. The flag-shape hysteretic behavior of superelastic SMA is a direct result of a reversible stress-induced phase transformation between austenite and martensitic phases. It is notable that the coupling between SMA bar and steel bar is assumed as perfect without slippage during loading. Such assumption neglects the energy dissipation locally occurred in the coupling of SMA and steel bars. The wide exploration of

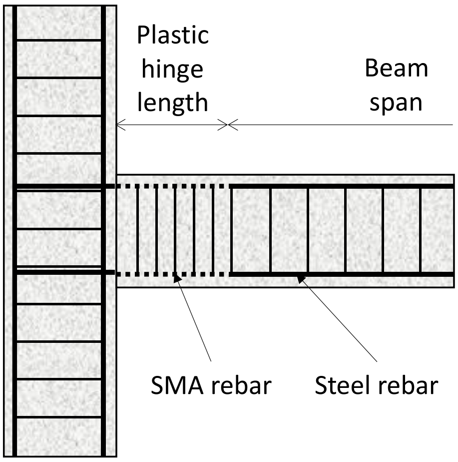

Fig. 1 Schematics of MRF configuration utilized in numerical modeling

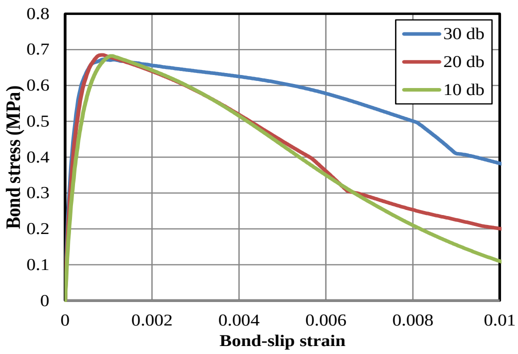

Fig. 2 Comparison of stress strain curves of experiment and numerical model for SMA material

the slippage response of SMA and steel bars can be found in recent works of Alam *et al.* (2010). The results of the mentioned study show that commercially available screw-lock couplers are found to be unsuitable for connecting SMA to steel bars. Furthermore, an existing coupler has been modified for SMA–steel splicing to allow SMA bars to achieve their full superelastic strain.

The influence of bond on performance at the strain distribution and on the rotation capacity is represented by a modification of the tension stiffening from surrounding concrete. The bond stress-slip relationship depends on a considerable number of influencing factors like rib geometry (related rib area), concrete strength, position and orientation of the bar during casting, state of stress, boundary conditions and concrete cover (Model Code 2010). The bond stress-slip curve for unconfined concrete can be considered as statistical mean curves, applicable as an average formulation for a broad range of cases. With this option the concrete is defined with solid elements and the rebar elements, each with their own unique set of nodal points. A string of spatially consecutive nodes, called slave nodes, related to the truss elements may slide along another string of spatially consecutive nodes, called master nodes, related to the solid elements. The sliding commences when the rebar debonds. The bond between the rebar and concrete is assumed to be elastic perfectly plastic. The maximum allowable slip strain, $u_{\max}$, is given as

$$u_{\max} = s_{\max} e^{-\alpha D} \tag{1}$$

where D is the damage parameter $D_{n+1}=D_n+\Delta u$. The shear force, acting on area A_s, at time n+1 is given as

$$f_{n+1} = \min\left\{ f_n - G_B A_s \Delta u, G_B A_s u_{\max} \right\}. \tag{2}$$

where G_B is the bond shear modulus, A_s is the area of the rebar, α is the exponent in the damage curve. The bond stress versus slip strain for the concrete of 53.5 MPa crushing strength of the reference experimental work (Youssef *et al*. 2008) is plotted in Fig. 2.

2. Nonlinear simulation of RC joint

In the present study, finite element method (FEM) analysis of the models was carried out using LS-DYNA environment. The interest in connection modeling is on load-drift properties and the onset of cracking. The concrete modeling was performed using solid 8-node elements with three degrees of freedom for each node and full Gaussian integration. The required properties for the material constitutive models were extracted from the stress-strain and strain-drift relations. In reinforced concrete modeling, enhanced selective/reduced (S/R) solid formulation is used, which resolved the shear locking phenomenon and improved the prediction accuracy of drifts and stresses. The S/R solid formulation has features as (1) selective reduced integrated brick element; (2) no hourglass stabilization needed; and (3) accurate formulation for explicit procedure with high computational cost. The Beam elements offered by LS-DYNA were used to model the bars. Among the three beam elements offered by LS-DYNA, the Hughes-Liu beam type with section integration was considered as the suitable element for simulation of reinforcement in this study (Kyei 2014). In this study, the material model MAT_84 known as Winfrith concrete is used to simulate the concrete material. In 1980 this concrete model expanded and used in concrete structures which were subjected to impact. This material model considers the strain-rate effect and tension softening which is handled in a different way than the compression. Basic plasticity model contains third constant stress for compatibility with tension and three axis pressure. The plasticity portion of the Winfrith concrete model is based upon the shear failure surface (Ottosen 1977)

$$F\left(I_1, J_2, \cos(3\theta)\right) = a\frac{J_2}{\left(f_c'\right)^2} + \lambda\frac{\sqrt{J_2}}{f_c'} + b\frac{I_1}{f_c'} - 1 \tag{3}$$

The above is referred to as a four parameter model: the constants a and b which control the meridional shape of the shear failure surface, and $\lambda=\lambda\cos(3\theta)$ ranging for $-1\leq\cos(3\theta)\leq1$ triaxial compression to triaxial extension control the shape of the shear failure surface on the π-plane with limits $0\leq\theta\leq/\pi3$. In addition to an explicit dependence on the unconfined compressive strength, f_c', the constants a and b also depend on the ratio of the unconfined tensile strength, f_t', to the unconfined compressive strength. Here, I_1 is the first invariant of Cauchy's stress tensor, J_2 is

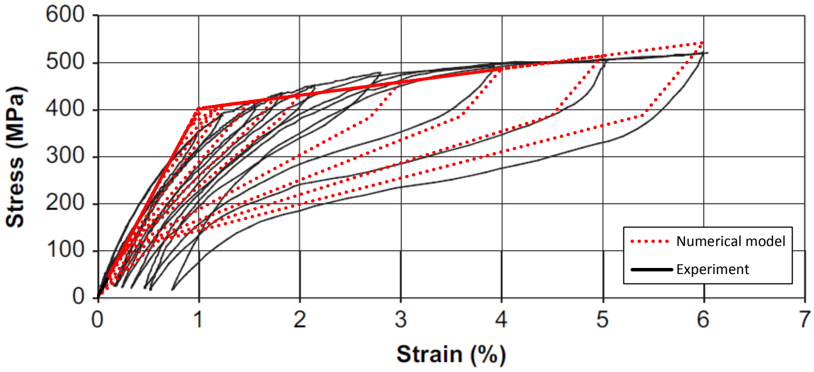

Fig. 3 The stress strain curves of experiment and numerical model for SMA material (Youssef *et al.* 2008)

the second invariant of the deviatoric stress tensor, and $\cos(3\theta)=3\sqrt{3}J_3/2J_2^{1.5}$ where J_3 is the third invariant of the deviatoric stress tensor. For normal strength concrete, dimensionless factors are calibrated as α=1.16, β=0.591, and γ=−0.612 where the constants a and b would be evaluated as

$$b=\frac{1+R\alpha\frac{\gamma}{3}-\alpha^2\frac{\gamma}{3}-\frac{\alpha}{R}}{\alpha^2\frac{\beta}{3}-3\alpha-R\alpha\frac{\beta}{3}},a=\beta b+\gamma \tag{4}$$

where $R=f_t'/f_c'<1$ is the ratio of the unconfined tensile to compressive strengths. The main features of the Winfrith concrete are as (1) a basic plasticity model that includes the third stress invariant for consistently treating both triaxial compression and triaxial extension, e.g., Mohr-Coulomb like behavior; (2) uses radial return which omits material dilation, and thus violates Drucker's Postulate for a stable material; (3) includes strain softening in tension with an attempt at regularization via crack opening width, fracture energy, and aggregate size; (4) concrete tensile cracking with up to three orthogonal crack planes per element; and (5) optional inclusion of smeared reinforcement.

The software includes two material models for the longitudinal and transversal steel bars, between which the MAT-3 plastic kinematic model was used as a suitable model for these materials. To develop stress–strain models of the SMA, fiber section approach was used. In addition, the bonding behavior of the SMA rebar is assumed as the developed bond-slip response where the rebar is ribbed with the surface friction adhesion to the concrete. The SMA uniaxial material model available as MAT-30 in material library was used to represent the behavior of SMA wire. Fig. 3 shows comparison of experimental results obtained from Yousef *et al*. (2008) work and numerical model results SMA material. Results show that the numerical models are able to depict the initial modulus and strength characteristics in addition to hysteretic behavior and accumulated residual strains of the SMA for different strain levels. Numerical models are also able to capture the forward and reverse transformation associated with change of phase in SMA material. The assumption that the developed constitutive models are able to numerically predict behavior of SMA is qualified notion as the models

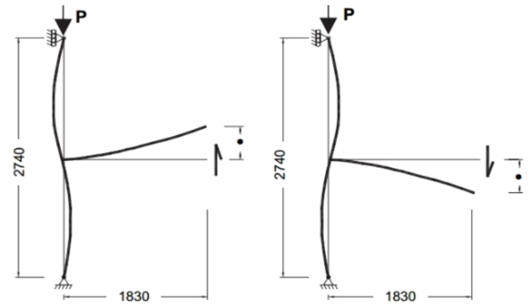

Fig. 4 Deformed sample along with the boundary conditions considered for the connection (Youssef *et al*. 2008)

are able to capture the section stiffness along with forward and reverse transformation associated with change of phase in SMA material. Because of compliance of numerical models with experimental results, calibrated SMA material model were incorporated in SMA reinforced structural frame models for cyclic analysis.

To apply the required boundary conditions, it is essential to use loading plates in order to prevent stress concentration and closely simulate laboratory conditions. The meshing layout in load plates is similar to that of the transversal column-beam section and hence exhibits a merged behaviour with the concrete at their intersection points. A rigid material with higher stiffness, relative to other materials, was set for the loading plate for proper and fixed load transfer. The boundary condition for the lateral connections was considered two pinned hinges at the bottom and top of the column, such that the column was allowed to rotate around Y axis. Deformation of the beam ends was prevented along the x and z axes. Fig. 4 shows the boundary conditions for the connection.

A suitable interaction should be defined between the concrete and steel. A part of these interactional effects is considered in the definition of concrete tensile hardening. However, a suitable relationship should be defined between concrete and steel in LS-DYNA. It is obvious that the degree of freedom of bars should not be independent of the degree of freedom of the surrounding concrete. To this end, LS-DYNA was equipped with Lagrangian-in-solid capability. This capability allows for embedding a part inside another, such that the degree of freedom of the internal part can be interpolated using the degree of freedom of its container. This capability forms a slave (steel

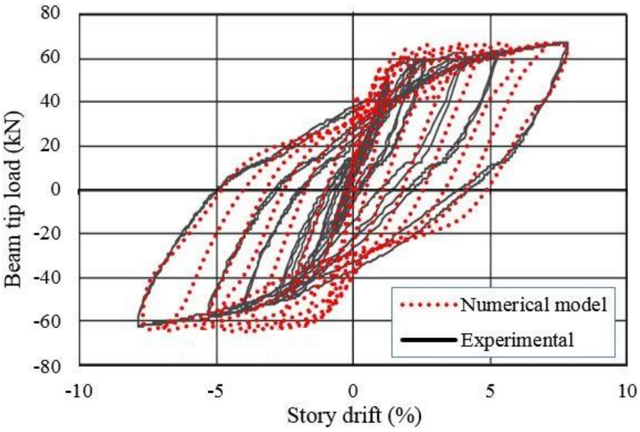

Fig. 5 Comparison of load-drift curve of numerical and laboratory results for JBC-1 sample

or bar) and host (concrete) state for two connected elements. The number of elements up to which the degree of freedom of the internal parts affects that of the external parts should be set. In this study, this number was regarded as one element because the bars were only involved with their surrounding concrete, and thus its degree of freedom should be linked only with that of the adjacent concrete (Hawileh *et al*. 2010). Therefore, the total number of converged and verified solid concrete elements and link rebar elements are 29440 and 1420, respectively.

3. Validating seismic behavior of RC connection

This part aimed at modeling the RC beam-column connection using LS-DYNA and then validating it through comparison with previous laboratory results. For validation, the laboratory sample from the work of Yousef *et al*. (2008), including the two following connections, was modeled.

3.1 Connection with ordinary bars (JBC-1)

This connection included a column with dimension of 400×250 mm, four bars with a diameter of 20 mm as the longitudinal bars, and some stirrups with diameter of 10 mm, spacing of 80 mm and 115 mm within and outside the critical region of the column, respectively. The beam connected to the column with dimension of 400×250 mm had four bars with diameter of 20 mm as the longitudinal bars, and stirrups of 10 mm with a spacing of 80 mm and 120 mm within and outside of the critical region, respectively. The compressive and tensile strengths of the concrete for this connection were 53.5 MPa and 3.5 MPa, respectively. The elastic modulus, yield strength, and ultimate strength of the longitudinal bars were 198 GPa, 520 MPa, and 630 MPa, respectively. Additionally, the yield and ultimate strengths of the transversal bars were 422 MPa and 682 MPa, respectively. According to the laboratory results, the shear failure in the control sample occurred at the side of the connection, as well as a part of the panel zone. The load-drift curves were extracted from numerical results. The experimental yield load is reported as 60 kN

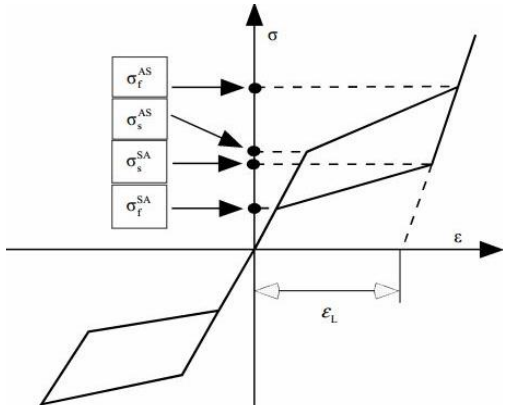

Fig. 6 The stress-strain curve of SMA material

which is not symmetric in the load-unload paths. However, the numerical obtained corresponding point is estimated as 65 kN with 8.5% over estimation relative error. Furthermore, the unloading paths are stiffer in numerical model than the experimental case, due to local buckling of the rebar denoted in experiment as shown in Fig. 5.

3.2 Connection with SMA-based bars (JBC2)

The second connection was exactly similar to the first one, except that four SMA-based bars with a coupler connection were used instead of the ordinary bars in the panel zone. The SMA-based bars are replaced with the steel ones in the length of 1.5 times the effective depth of the beam adjacent to the panel zone (l_{SMA}=600 mm) both in the top and bottom of the section. Furthermore, the diameter of the SMA bars is 20 mm, exactly the same as the steel one. The compressive and tensile strengths of the concrete for this connection were 53.7 MPa and 2.8 MPa, respectively. The elastic modulus, yield strength, and ultimate strength of the longitudinal bars were 193 GPA, 450 MPa, and 650 MPa, respectively. The SMA-based bars acted differently from ordinary bars, exhibiting a flag-shaped behavior in the stress-strain curve as compared to the steel bars as shown in Fig. 6. The Poisson's ratio for SMA-based bars was 0.33. The parameter α indicates the difference between the tensile and compressive stresses, which is known as Bauschinger effect. The expression for backward coefficient α is expressed as Eq. (5).

$$\alpha = \frac{\sigma_s^{AS,-} - \sigma_s^{AS,+}}{\sigma_s^{AS,-} + \sigma_s^{AS,+}} \tag{5}$$

In addition ε_L is the maximum strain in the strain-stress curve. Extracted from the numerical results, the load-drift curve and the energy curve were appropriately consistent with the experimental results in the linear, nonlinear, and hardening regions of steel as shown in Fig. 7.

The slight difference between the curves (4%) was due to the heterogeneous behavior of concrete during loading, considering an ideal geometry and interaction between the members, and the fact that mechanical connections were not used in the numerical models. A summary of the comparison between experimental and numerical results is presented in Table 1.

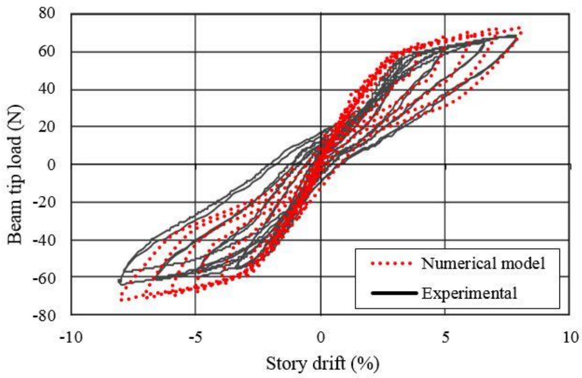

Fig. 7 Comparison of load-drift curve of numeric and experiment results of JBC-2 sample

Table 1 Results from analysis of validated samples

Model Number	Ultimate Load (kN)		Residual Force (kN)		Dissipated Energy (kN.m)		Residual Drift (%)	
	Exp.	Num.	Exp.	Num.	Exp.	Num.	Exp.	Num.
JBC-1	66	63.18	38	34.3	26.4	25.5	4.2	5
JBC-2	67.5	70.9	16.5	12.9	16.8	15.9	0.95	1

It is significantly notable that the difference between numerical and experimental results of the hardening branch of the drift-load curve is due to the idealized assumption of the slippage phenomenon occurring in the coupling of SMA and steel bars. Under laboratory conditions, there exist slippage and bonding loss between SMA and steel which results in strength loss in the coupling zone of two materials. However, such phenomenon does not occur in the numerical model due to the perfect bonding of the two bar types. Therefore, it is important to practical use to consider the bonding loss of SMA and steel bars in the coupling zone to make more accurate results.

4. Parametric studies

The samples under investigation were different in reinforcement details and the percent of longitudinal bars in the beam. Different amounts of SMA were used as longitudinal bars in the seven QBIM samples. Connections in this part were similar to laboratory samples in terms of model geometry, boundary conditions, and loading. Details of the models are presented in Table 2. It should be noted that the effect of the temperature the possible influence of temperature on the behavior of samples with SMA bars is neglected in the current study for simplification of analyses.

4.1 Moment-rotation curves

The beam moment-rotation curves for the QBIM samples are presented in Fig. 8. According to these diagrams, by increasing the percentage of SMA bars and subsequently reducing the steel bars amount, the pinching in the moment-rotation curves increased. On the other hand, the ductility and energy absorption of the samples reduced. The plastic rotation of the QBIM1 is estimated as 0.055 radians while the plastic rotation of the QBIM7 is 0.005 radians where it is reduced by 11 times. Furthermore, the plastic rotation of QBIM3 and QBIM5 are 0.045 and 0.03 radians, respectively. Results show that higher amount of SMA bars decrease effectively the plastic rotation while lower amount of SMA bars result in more efficient decrease of dissipated energy. However, due to analogous strength of SMA and steel rebar, the ultimate capacity of connection in the numerical model was approximately 160 kN.m.

4.2 Energy dissipation and secant stiffness curves

Figs. 9 and 10 show, respectively, the energy dissipation curve obtained from calculation of the area under the load-displacement curve and the secant stiffness curve obtained from division of load by drift for all the seven connection samples. According to Fig. 9, the maximum energy dissipation was observed in the sample with 100% steel bars (QBIM1). The energy dissipation for this sample was 29kN.m. The lowest energy absorption was 6.5 kN.m in QBIM7, which contained the highest percentage of SMA. This value was 75% lower than the highest value. It can be

Table 2 Reinforcement details of SMA reinforced RC joints

Model	Column reinforcement		Beam Reinforcement				
	Rebar	Stirrup	Longitudinal rebar				Stirrup
		Hinge Zone	Steel		SMA		Hinge Zone
		Rest of Member	Detail	Percentage	Detail	Percentage	Rest of Member
QBIM1	4Φ20	Φ10@80 Φ10@115	4Φ16(bottom) 4Φ16(Top)	100	-	0	Φ10@80 Φ10@120
QBIM2	4Φ20	Φ10@80 Φ10@115	2Φ20(bottom) 2Φ20(Top)	75	2Φ12(bottom) 2Φ12(Top)	25	Φ10@80 Φ10@120
QBIM3	4Φ20	Φ10@80 Φ10@115	2Φ18(bottom) 2Φ18(Top)	65	2Φ14(bottom) 2Φ14(Top)	35	Φ10@80 Φ10@120
QBIM4	4Φ20	Φ10@80 Φ10@115	2Φ16(bottom) 2Φ16(Top)	50	2Φ16(bottom) 2Φ16(Top)	50	Φ10@80 Φ10@120
QBIM5	4Φ20	Φ10@80 Φ10@115	2Φ14(bottom) 2Φ14(Top)	35	2Φ18(bottom) 2Φ18(Top)	65	Φ10@80 Φ10@120
QBIM6	4Φ20	Φ10@80 Φ10@115	2Φ12(bottom) 2Φ12(Top)	25	2Φ20(bottom) 2Φ20(Top)	75	Φ10@80 Φ10@120
QBIM7	4Φ20	Φ10@80 Φ10@115	-	0	4Φ16(bottom) 4Φ16(Top)	100	Φ10@80 Φ10@120

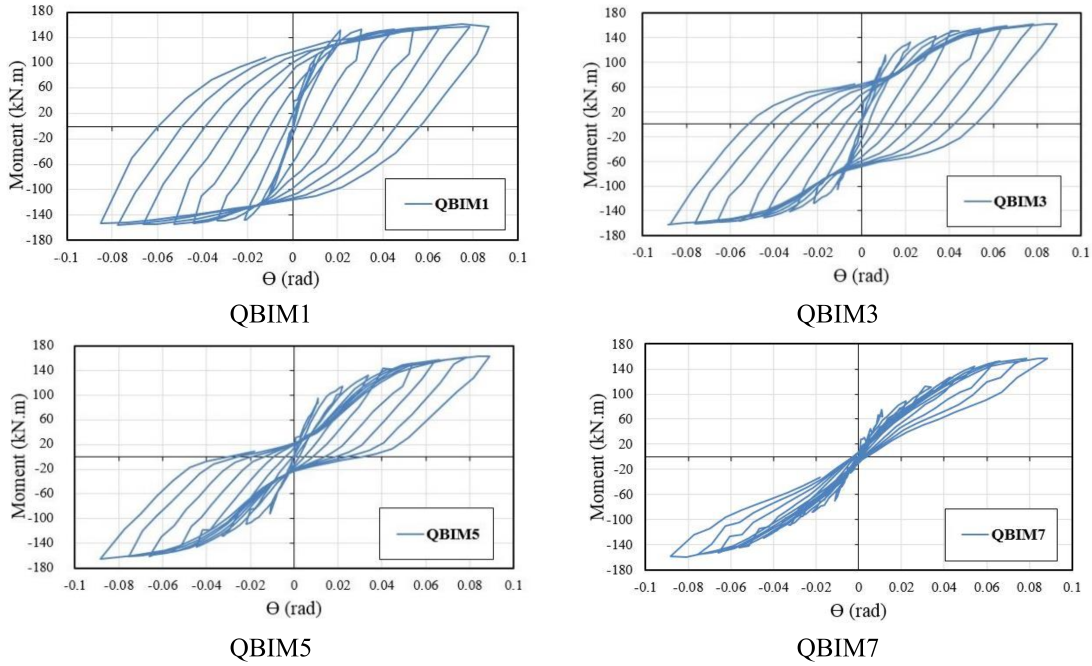

Fig. 8 Beam moment-rotation diagram of models with SMA joint bars

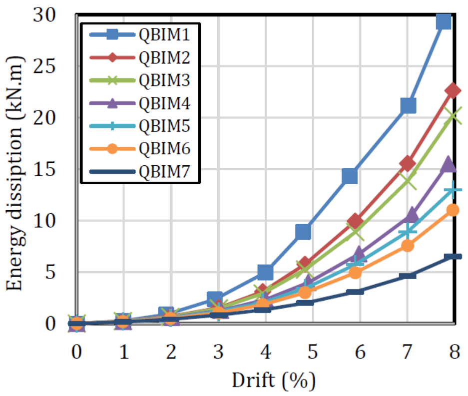

Fig. 9 Energy dissipation diagram of QBIMs

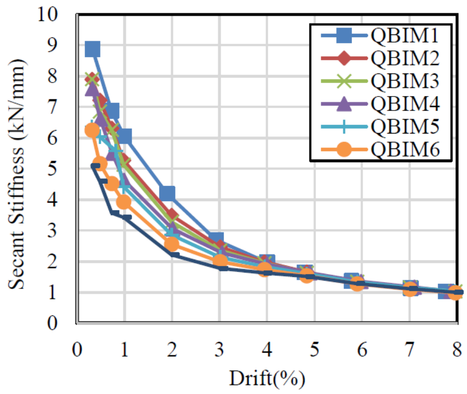

Fig. 10 Secant stiffness diagram of QBIMs

Table 3 Results of modeled SMA reinforced RC joints

Model	Rebar Percentage	SMA (%)	Ultimate Force (kN)	Residual Plastic rotation (rad)	Residual Force (kN)	Dissipated Energy (kN.m)
QBIM1	100	0	156.8	0.056	115.7	29
QBIM2	75	25	158.11	0.052	81.5	22.6
QBIM3	65	35	161.3	0.05	60.31	20.5
QBIM4	50	50	161.3	0.045	37.49	15.5
QBIM5	35	65	159.7	0.031	25.9	13
QBIM6	25	75	154.8	0.015	17.9	11.02
QBIM7	0	100	154.8	0.0032	5.5	6.5

concluded that energy dissipation reduces in proportion to the amount of increase in the employed SMA, which is not a desirable effect. To solve this problem, a suitable combination of SMA and steel is recommended.

The highest secant stiffness was 8.8kN.mm which was obtained for sample QBIM1. This stiffness was reduced by increasing the percentage of SMA, such that the lowest secant stiffness was 5.1 kN.mm obtained for sample QBIM7. According to the Fig 10, connection stiffness significantly reduces by increasing the percent of SMA, which can be attributed to the narrow hysteresis curve of such connections. Results for the other samples are summarized in Table 3.

4.3 Strain curves of bars

The strain values for a limited length of the connection bars were extracted. In this section, the bar strain at a distance of 50 mm from the connection side, along which plastic hinge formation is more likely, was obtained for QBIM1, QBIM4, and QBIM7, and results were presented in Fig 11 and Fig 12. According to these diagrams, the strain increased with increasing the percent of SMA-based bars in the connection side, such that the residual strain in QBIM1 was considerably higher than the other two samples. In QBIM7, no significant residual strain was observed in the connection side. Nevertheless, if we consider the probability of plastic hinge formation proportional to the degree of residual strain, it can be said that the plastic hinge moves away from the core by increasing the percent of

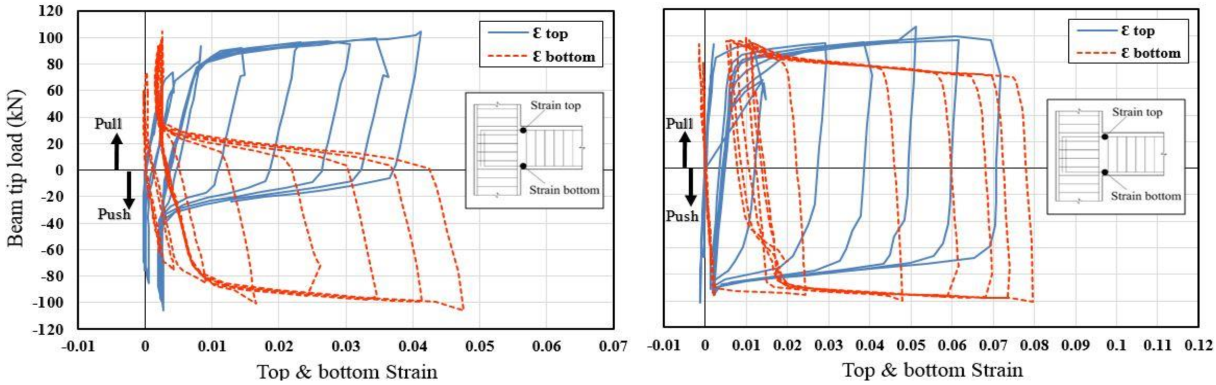

Fig. 11 Strain diagram of the bars in sample QBIM1 (right) and QBIM4 (left)

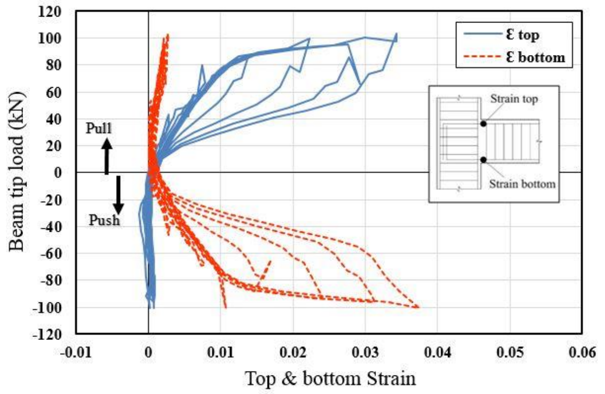

Fig. 12 Strain diagram of the bars used in sample QBIM7

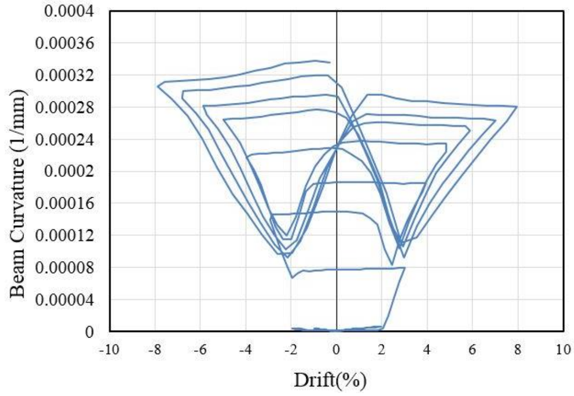

Fig. 13 Beam drift-rotation diagram in sample QBIM1

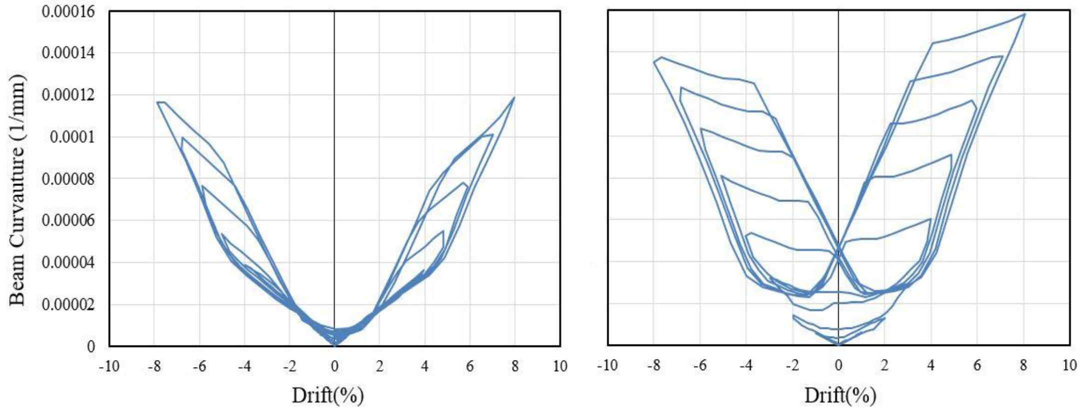

Fig. 14 Beam drift-curvature diagram for samples QBIM4 (right) and QBIM7 (left)

SMA. As a result, in QBIM1, the plastic hinge was near the connection core, but gradually moved away from the panel zone in QBIM4 and QBIM7.

4.4 Drift-curvature diagrams of the beams

The beam curvature, which indicates the rotation of a beam, is presented in the Fig. 13 and Fig. 14 for samples QBIM1, QBIM4, and QBIM7. The degree of curvature is obtained through dividing the sum of upper and lower strains of bars by the beam height in the connection side. These values appropriately represent the mechanism of plastic hinge formation. The beam curvature on the connection side was maximized in the sample with the highest amount of steel (QBIM1). However, it significantly reduced with increasing SMA-based materials in samples QBIM4 and QBIM7. As a result, the curvature or rotation of the beam decreased on the connection side by increasing SMA-based materials, meaning that the plastic hinge moved away from the column in these samples. According to the results, we can properly move the plastic hinge away from the connection core and the column and move it closer to the beam by increasing the SMA materials. This finding can be confirmed by the crack growth modes extracted from LS-DYNA. For examples, as shown in Fig. 15, the cracks can be observed in the panel zone of QBIM1, but the major cracks in sample QBIM7 are formed in the beam. It is notable that the cracks are demonstrated in pull cycle while

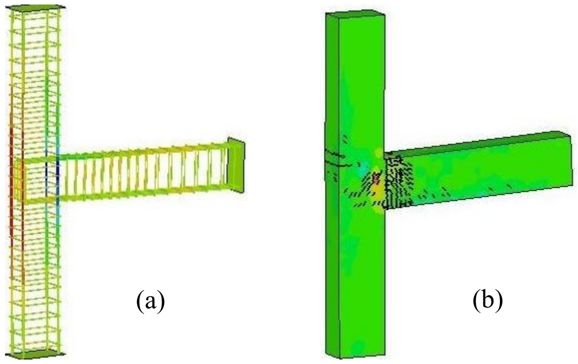

Fig. 15 (a) distribution of axial load of bars (b) cracking mechanism of QBIM1

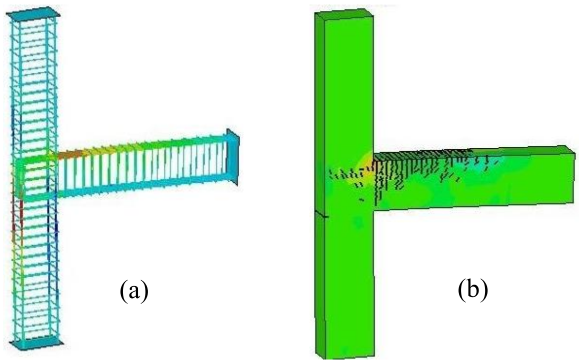

Fig. 16 (a) distribution of axial load of bars (b) cracking mechanism of QBIM7

the compressive cracks are closed and therefore cracks are concentrated in one side of the section.

5. Conclusions

This study investigated the performance of RC beam-column connections and correction of their behaviour using SMA-based materials. The following results were obtained from the analyses:

1. Comparative study into laboratory findings showed that LS-DYNA is capable of modelling such systems, such that the results were well consistent with the laboratory results in the linear, nonlinear, and strain hardening regions of steel.
2. The application of SMA-based bars, as the main bars, considerably contributes to the elimination of residual plastic rotations and reducing the need for repair after large earthquakes. On the other hand, the flag-shaped strain-stain curve of SMA-based bars results in slight residual deformation in SMA-based column-beam connections as compared to steel connections.
3. Significant reduction in residual plastic rotations and residual moment, along with an increase in pinching in the hysteresis curve of connections are among the advantages of SMA-based bars.
4. In SMA-based connections, the plastic hinge moves desirably away from the panel zone and approaches the beam. However, in steel connections, the plastic hinge is very close to the panel zone.
5. Results show lower energy dissipation in SMA-based materials than steel materials, which can be regarded as one of their disadvantages. However, a good combination of SMA-based bars and steel bars can improve this problem.

It should be noted that the connection between steel and SMA bars is an important issue and it is necessary to conduct several studies on the anchorage of SMA bars to steel ones to avoid local ruptures and possible damages prior to seismic performance demand.

References

Abdulridha, A., Palermo, D., Foo, S. and Vecchio, F.J. (2013), "Behavior and modeling of superelastic shape memory alloy reinforced concrete beams", *Eng. Struct.*, **49**, 893-904. https://doi.org/10.1016/j.engstruct.2012.12.041.

Alam, M.S., Moni, M. and Tesfamariam, S. (2012), "Seismic over-strength and ductility of concrete buildings reinforced with superelastic shape memory alloy rebar", *Eng. Struct.*, **34**, 8-20. https://doi.org/10.1016/j.engstruct.2011.08.030.

Alam, M.S., Youssef, M.A. and Nehdi, M. (2008), "Analytical prediction of the seismic behavior of superelastic shape memory alloy reinforced concrete elements", *Eng. Struct.*, **30**(12), 3399-3411. https://doi.org/10.1016/j.engstruct.2008.05.025.

Alam, M.S., Youssef, M.A. and Nehdi, M.L. (2010), "Exploratory investigation on mechanical anchors for connecting SMA bars to steel or FRP bars", *Mater. Struct.*, **43**(1), 91-107. https://doi.org/10.1617/s11527-010-9601-0.

Billah, A.M. and Alam, M.S (2012), "Seismic performance of concrete columns reinforced with hybrid shape memory alloy (SMA) and fiber reinforced polymer (FRP) bars", *Constr. Build. Mater.*, **28**(1), 730-742. https://doi.org/10.1016/j.conbuildmat.2011.10.020.

Chalioris, C.E., Favvata, M.J. and Karayannis, C.G. (2008), "Reinforced concrete beam-column joints with crossed inclined bars under cyclic deformations", *Earthq. Eng. Struct. Dyn.*, **37**(6), 881-897. https://doi.org/10.1002/eqe.793.

DesRoches, R., McCormick, J. and Delemont, M. (2004), "Cyclic properties of superelastic shape memory alloy wires and bars", *J. Struct. Eng.*, **130**(1), 38-46. https://doi.org/10.1061/(ASCE)0733-9445(2004)130:1(38).

Du Béton, F.I. (2010), "Model code 2010-First complete draft", *FIB Bull.*, **55**, 318.

El-Amoury, T. and Ghobarah, A. (2002), "Seismic rehabilitation of beam-column joint using GFRP sheets", *Eng. Struct.*, **24**(11), 1397-1407. https://doi.org/10.1016/S0141-0296(02)00081-0.

Georgiades, A.V., Saha, G.C., Kalamkarov, A.L., Rokkam, S.K., Newhook, J.P. and Challagulla, K.S. (2005), "Embedded smart GFRP reinforcements for monitoring reinforced concrete flexural components", *Smart Struct. Syst.*, **1**(4), 369-384. https://doi.org/10.12989/sss.2005.1.4.369.

Ha, G.J., Kim, J.K. and Chung, L. (1992), "Response of reinforced high-strength concrete beam-column joints under load reversals", *Mag. Concrete Res.*, **44**(160), 175-184. https://doi.org/10.1680/macr.1992.44.160.175.

Hawileh, R.A., Rahman, A. and Tabatabai, H. (2010), "Nonlinear finite element analysis and modeling of a precast hybrid beam–column connection subjected to cyclic loads", *Appl. Math. Model.*, **34**(9), 2562-2583. https://doi.org/10.1016/j.apm.2009.11.020.

Kabir, M.R., Alam, M.S., Said, A.M. and Ayad, A. (2016), "Performance of hybrid reinforced concrete beam column joint: A critical review", *Fiber.*, **4**(2), 13. https://doi.org/10.3390/fib4020013.

Kyei, C. (2014), “Effects of blast loading on seismically detailed reinforced concrete columns”, Doctoral Dissertation, Carleton University.

Li, B. and Kulkarni, S.A. (2009), “Seismic behavior of reinforced concrete exterior wide beam-column joints”, *J. Struct. Eng.*, **136**(1), 26-36. https://doi.org/10.1061/(ASCE)0733-9445(2010)136:1(26).

Masi, A. and Santarsiero, G. (2013), “Seismic tests on RC building exterior joints with wide beams”, *Adv. Mater. Res.*, **787**, 771-777. https://doi.org/10.4028/www.scientific.net/AMR.787.771.

Masi, A., Santarsiero, G. and Lignola, G.P.M. (2013), “Study of the seismic behavior of external RC beam–column joints through experimental tests and numerical simulations”, *Eng. Struct.*, **52**, 207-219. https://doi.org/10.1016/j.engstruct.

Nehdi, M., Alam, M.S. and Youssef, M.A. (2011), “Seismic behaviour of repaired superelastic shape memory alloy reinforced concrete beam-column joint”, *Smart Struct. Syst.*, **7**(5), 329-348. https://doi.org/10.12989/sss.2011.7.5.329.

Ottosen, N.S. (1977), “A failure criterion for concrete”, *J. Eng. Mech. Div.*, **103**(4), 527-535.

Qissab, M. and Salman, M.M. (2018), “Shear strength of non-prismatic steel fiber reinforced concrete beams without stirrups”, *Struct. Eng. Mech.*, **67**, 347-358. https://doi.org/10.12989/sem.2018.67.4.347.

Rezaee Azariani, H., Esfahani, M.R. and Shariatmadar, H. (2018), “Behavior of exterior concrete beam-column joints reinforced with Shape Memory Alloy (SMA) bars”, *Steel Compos. Struct.*, **28**(1), 83-98. https://doi.org/10.12989/scs.2018.28.1.083

Santarsiero, G. (2018), “FE modelling of the seismic behavior of wide beam-column joints strengthened with CFRP systems”, *Build.*, **8**(2), 31. https://doi.org/10.3390/buildings8020031.

Shahverdi, M., Czaderski, C., Annen, P. and Motavalli, M. (2016), “Strengthening of RC beams by iron-based shape memory alloy bars embedded in a shotcrete layer”, *Eng. Struct.*, **117**, 263-273. https://doi.org/10.1016/j.engstruct.2016.03.023.

Wang, X., Zhou, C., Ai, J., Petru, M. and Liu, Y. (2020), “Numerical investigation for the fatigue performance of reinforced concrete beams strengthened with external prestressed HFRP sheet”, *Constr. Build. Mater.*, **237**, 117601. https://doi.org/10.1016/j.conbuildmat.2019.117601.

Youssef, M.A., Alam, M.S. and Nehdi, M. (2008), “Experimental investigation on the seismic behavior of beam-column joints reinforced with superelastic shape memory alloys”, *J. Earthq. Eng.*, **12**(7), 1205-1222. https://doi.org/10.1080/13632460802003082.

CC